

## Influence of carbonitriding on microstructure, residual stress and mechanical properties of graded cemented carbides

Man Feng Gong<sup>a,b</sup>, Jian Chen<sup>a,\*</sup>, Qiang Guo Jiang<sup>a</sup> and Shang Hua Wu<sup>a,\*</sup>

<sup>a</sup>College of Electro-mechanical Engineering, Guangdong University of Technology, Guangzhou, China

<sup>b</sup>Dept. of Mechano-electronic, Lingnan Normal University, Zhanjiang, Guangdong Province, P.R. China

The influences of carbonitriding treatment on the microstructure, residual stress and mechanical properties of Ti-containing cemented carbides are investigated. Three powder compacts of WC-7.0Co-2.0Ni-3.0Mo-0.5TiC cemented carbides were liquid phase sintered in vacuum at 1,300 °C for 1h. Three specimens with cobalt-enriched surface layers were obtained. They were subsequently carbonized by a post-sintering heat treatment process in nitrogen. The carbonitriding treatment results in the formation of fine-grained TiN phases and N-diamond C phases in situ on their surfaces. X-ray diffraction spectrums reveal their differences in the grain size and forming phases of the Ti-containing phases for cemented carbides before and after carbonitriding treatment. This method can reduce the grain size of Ti-containing hard phase and increase microstrains in it. To analyze the residual stress, the specimen before and after carbonitriding was measured by recording the peak positions for each  $2\theta$  at five different tilt angles ( $\psi = 0^\circ, 20.7^\circ, 30^\circ, 37.8^\circ$  and  $45^\circ$ ) by a X-ray diffractometer. The microstructure and defects of cemented carbides were investigated by SEM before and after the carbonitriding treatment. It is concluded that: (1) high bond strength between the Ti-containing skin and the WC-Co substrate, (2) high wear resistance of the Ti-containing skin after carbonitriding, (3) compression stress state existing in Ti-containing skin, (4) the technology of carbonitriding treatment contributes to form an aesthetic Ti-containing skin in the surface of cemented carbides and improve its wear resistance.

**Key words:** FG WC-Co, Ti-containing skin, Carbonitriding treatment, Residual stress, Wear resistance.

### Introduction

Cemented carbides are hard metal alloys, used for e.g. cutting, turning and drilling of metals, or moulds such as casting dies and abrasive tools. The material consists of one or more hard carbide phases and a more ductile metallic binder phase. The amount of binder phase can vary depending on application fields for the cemented carbides, but it is usually less than 15 vol. % [1]. For many applications WC-Co is not hard or wear resistant enough, so second hard carbide with cubic phase is introduced. The most common refractory metal carbide hard phase in cemented carbides is WC. Depending on the application and properties required, other refractory carbides such as TiC, TaC, Cr<sub>2</sub>C<sub>3</sub>, Mo<sub>2</sub>C, SiC and NbC are added as hard phases [2-5]. In cemented carbides, mostly Co is used as binder phase because of its superior mechanical properties in combination with good wettability and adhesion to the hard phases [6]. In applications requiring increased corrosion resistance, the use of Ni, Co/Ni or even Co/Ni/Fe complex binders can be favorable [7, 8]. Further increase in wear resistance and, hence, in the tool life is often achieved by depositing hard coatings (e.g. TiC,

TiN, Ti(C, N) or Al<sub>2</sub>O<sub>3</sub>) on the cemented carbides [9-12]. Due to differences in thermal expansion coefficient between coatings and substrates, microcracks will unavoidably form in the coatings. When the inserts are used for machining other metal materials, these microcracks might propagate into the substrate and cause failure. Compared to homogeneous WC-Co, FG WC-Co has been found to be able to offer superior combinations of wear resistance and fracture toughness [13-15]. Therefore, many processes have been developed to produce FG WC-Co with various types of graded structures [16-18]. In order to study the effect of carbon on gradient surface zone formation and increase crack propagation resistance in cemented carbides, a so-called gradient sintering was used to product these cutting tools with tough surface zones [1]. In this sintering process TiN-containing cemented carbide was sintered in a nitrogen free atmosphere. The results reveal that the difference in nitrogen activity between atmosphere and cutting tool during sintering will create outward nitrogen diffusion. Due to thermodynamical coupling between nitrogen and titanium, this gives rise to an inward titanium diffusion, which creates a surface zone depleted of hard cubic phases and enriched in ductile binders. By sintering cemented carbides at different carbon activities, it was found that the average WC grain size increased and the grain size distribution became slightly wider with increasing C content [19]. Bounhoure *et al.* [20] revealed that while shrinkage and

\*Corresponding author:

Tel : +086-0759-3183184

Fax: +086-0759-3183046

E-mail: jianchen2014@126.com, swu@gdut.edu.cn

Co spreading started earlier in the W-enriched FG WC-Co alloy, the reduction of porosity and Co spreading was more uniform in the C-enriched FG WC-Co alloy. Baratti *et al.* [21] revealed that a high nitrogen activity leads to the preferred dissolution of the core-rim structure of the mixed cubic carbide grains, and it can be used to improve the wear and corrosion resistance of cemented carbides with both Co-binder and Ni-binder. Cheng *et al.* [22, 23] deposited TiCN coatings with different C content by using a large area filtered arc deposition (LAFAD) technique from Ti targets under the atmosphere of mixing N<sub>2</sub> and CH<sub>4</sub> gases. Mechanical results revealed that with increasing C content in the coatings, the hardness and elastic modulus increased to a maximum at a C content of 2.8 at.%, then decreased rapidly. A new procedure [5, 8] was developed to economically produce Co depleted WC-Co with gradient thicknesses ranging from tens to thousands of microns. Unlike in the DP carbide process, no brittle eta phase (Co<sub>3</sub>W<sub>3</sub>C) existed before the processing or forms during this process. Similarly, a novel carburizing process for manufacturing FG WC-Co was developed by Guo Jun and his coworkers [14]. In this process, the Co gradient was formed by heat treating conventional liquid-phase-sintered WC-Co in a carburizing atmosphere (CH<sub>4</sub>) at temperatures that allow three-phase equilibriums among solid WC, solid Co, and liquid Co. WC-10 wt.%Co specimen with a stoichiometric C content was to be carburized at 1300 °C. During the carburization process, the C content in the surface region increased, leading to the increase of the volume fraction of liquid Co phase in the surface region, and giving rise to the migration of the liquid Co phase from the surface region toward the core and thus resulting in the formation of Co gradient with reduced Co content in the surface region. A two-step process was developed in order to create thicker FG WC-Co [14]. The first step was to carburize the specimen at a temperature higher than the three-phase-region temperature, so the depth of C diffusion was large without causing significant changes to the volume fraction of liquid at the same time. The cobalt gradient was then formed in the second step by cooling and holding the sample at a temperature within the three-phase-region for a short period of time. In this way, the final depth of the Co gradient is expected to be equal to the relatively large depth of C diffusion.

A novel sintering process is applied to create a type of new functionally graded WC-Co in this study. In this process, Co gradient formation, C diffusion and Ti-containing coating creation are de-coupled from each

other. Finally, an aesthetic and Ti-containing hard skin on the surface of cemented carbide was successfully deposited in situ on their surfaces by a carbonitriding treatment process. The grain size and microstructure in/on specimen was observed by SEM, the compositions, phases and the residual stress were analyzed by XRD, and the wear resistance and friction coefficient was measured by friction and wear test.

## Experimental Details

WC, Co, Mo, Ni and TiC Powders are used to prepare the samples with a composition of WC-7.0Co-2.0Ni-3.0Mo-0.5TiC (wt.%). Raw powders were produced by the Shanghai Shuitian. Nanotech. Co. Ltd., and were fabricated by a catalytic pyrolysis of hydrocarbon technique. The composition of powders is following: WC (2 μm) with a C<sub>total</sub> of 5.72 ± 0.05 wt.%, TiC (1 μm) with a C<sub>total</sub> of 12.54 ± 0.05 wt.% and (Co, Ni, Mo) alloy powders 58/17/25 with a C<sub>total</sub> of 0.06 wt.%. Three metal powders, i.e. Co, Ni and Mo, are the fine powders (~ 1.0 μm) with quality containing 0.2% impurities. The compositions of raw powders are summarized in Table 1.

The dimensions of three raw powder compacts were 6.8 mm in height, 17.7 mm in width and 17.7 mm in length, and their average mass was about 13.71 g. Firstly, they were put into a high vacuum-brazing-furnace (its maximum vacuum degree was 5.0 × 10<sup>-4</sup>, TYQH-48, China), and then liquid-phase-sintered at 1300 °C for 1 h. This temperature should be kept within three-phase-region temperature range (1275-1325 °C) during the sintering process [14]. The three-phase-region corresponds to equilibriums among solid WC, solid Co, and liquid Co. The average dimensions of three as-sintering specimens were about 5.4 mm in height, 14.2 mm in width and 14.2 mm in length, and their average mass reduced to 13.49 g. The data of their volumetric shrinkage rate and weight loss rate were about 48.9% and 1.6%, respectively. Then we deliberately grinded off the Co-enriched layer on the specimens for a standard dimension of cutting tool (4.76 mm in height, 12.76 mm in width and 12.76 mm in length). The Ti-containing skin was prepared in the last step by a carbonitriding treatment process, in which the as-polished specimens were put into a graphite crucible and covered by graphite powers for carburizing in nitrogen and holding at 1300 °C for 30 min in an atmosphere furnace (ZT-90-22, China). Thus a brown Ti-containing skin was obtained on the in situ surface of specimen.

**Table 1.** Composition of raw powders.

Total carbon content (wt.%)	Free carbon content (wt.%)	Oxyger content (wt.%)	Co content (wt.%)	Mo content (wt.%)	Ni content (wt.%)	TiC content (wt.%)	W content (wt.%)
5.72	0.16	0.10	7.00	3.00	2.00	0.50	balance

The microstructures of specimens after sintering and prior to carbonitriding, as well as after carbonitriding, were observed by a scanning electron microscope (SEM, NOVA NANOSEM 430). The residual stress in the skin of specimens were measured by an X-ray diffractometers (X' Pert Pro MPD, PANalytical), and the compositions and phases generated in specimens were analyzed by an X-ray diffractometers (XRD, Bruker D8). A friction and wear tester (SRV-4, China) was applied for testing the friction coefficient and wear resistance of specimens.

## Results and Discussion

### Microstructure

Different processes result in different surface topographies and mechanical properties of cemented carbides. The typical surface appearance of no Co capping specimen, which is directly sintered in nitrogen, is shown in the Fig. 1 (a) and (a'). (a) shows the transverse section of the specimen, and (a') is the microstructure on the surface of specimen. There are some obvious defects such as cracks and pores appearing in the interior of specimen as shown in two figures. The average WC grain size is about 2  $\mu\text{m}$ , and the average surface roughness is about 4  $\mu\text{m}$ .

Its surface quality can be completely improved as a result of the Co-capping technology, which is clearly seen in Fig. 1 (b) and (b'). In our study, the Ti-

containing powder compacts were liquid phase sintered in vacuum at 1300 °C and held for 1 h. The Co capping layer was formed on the surfaces of specimens and featured that the Co content on the surface was higher than that of the interior region. Moreover, no cubic carbides (TiC, TiN and TiCN) existed in this region. The specimen sintered in vacuum appears a shiny surface, which attributes to the formation of a Co capping on the surface of specimen [17]. The Co capping technology was firstly reported in 1981 by Taniguchi *et al.* [24]. In many cases, the Co capping technology contributes to produce different gradients with continuous, fcc-free phases and shiny surfaces. The presence of Co capping on the surface of cemented carbide results in the dramatic improvements of their transverse rupture strength, surface fracture toughness and wettability by braze alloys [25]. However, it is usually considered undesirable and removed by machining following sintering. Although the Co capping phenomenon is discussed in many literatures, its mechanism is not well understood and is still arguing [26]. For examples, Taniguchi and the coworkers [24] thought that the phenomenon of forming Co capping and fcc-free surface was attributed to the Co liquid phase migration. They presented that Co-capping and Co enrichment occurred in the temperature range where solid and liquid Co coexisted, and the flow of liquid Co depended on the shrinking induced by the solidification of liquid Co. However, Janisch *et al.* [27] refuted that the above-mentioned mechanism could not be applicable to explain the formation of Co capping. They proposed a different mechanism, which is that the liquid Co in the interior region solidifies first before the liquid Co in the surface region does, and the solidification in the interior region exerts a compression on the surface region which is soaked with liquid Co, thus squeezing the liquid Co out to the surface. Sachet *et al.* [28] indicated that the high surface tension of liquid cobalt is responsible for the formation of the Co capping layer. The slightly decarburizing conditions during vacuum sintering can cause a transport of liquid cobalt towards the surface. Moreover, fast cooling or cooling under carburizing conditions can prevent the Co capping layer formation. Konyashin *et al.* [26] explained that the increased capillarity pressure results in the Co extrusion onto the surface. If the WC mean grain size in the hard-metal is small, the Co extrusion caused by the growing capillary pressures results in the Co penetration onto the surface of all WC grains and, as a result, the formation of a continuous Co film on the surface. Accompanying the consequent liquid volume increases in the surface layer of specimen, the inward Ti diffusion is driven by the outward binders (Co, Mo and Ni) diffusion. Through liquid migration, Co capping surface layer owning shiny metallic luster and relative smooth appearance can be obtained on the surface of specimen after sintering in vacuum. There

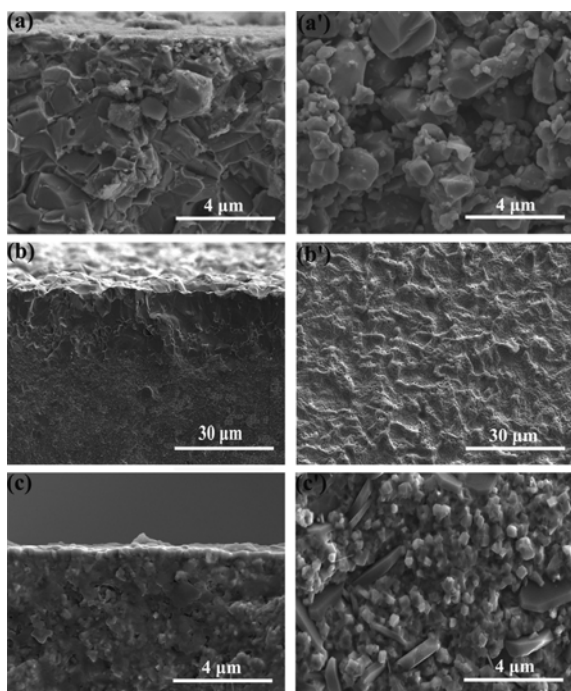


**Fig. 1.** Microstructure of specimen processed by different technologies, (a) Profile microstructure of no Co capping, (a') surface microstructure of no Co capping, (b) Profile microstructure of owning Co capping, (b') surface microstructure of owning Co capping, (c) Profile microstructure after carbonitriding treatment, (c') surface microstructure after carbonitriding treatment.

are two major advantages of the employment of the Co-capping technology tools not subjected to grinding. The first one is related to the fact that the surface of non-ground tools always comprises micro-cracks and other defects after sintering [29, 30], which can lead to a significant reduction of TRS and consequently performance properties [25]. Therefore, the Co-capping layer can completely “heal” such surface cracks and defects. Three specimens of as-sintering in vacuum were subsequently grinded into standard size, which is 4.76 mm in height, 12.76 mm in width and 12.76 mm in length. Their surface roughness results are less than 1  $\mu\text{m}$  (about 0.8  $\mu\text{m}$ ) after machining such as milling, polishing and chamfering. Three inserts appear shiny and their surface becomes smoother once the uppermost Co capping surface layers have been removed.

All specimens were then put into an atmosphere furnace to be further carbonitriding treatment. A type of fine-grained skin is formed on the surface of as-polished specimen after carbonitriding treatment as shown in Fig. 1(c) and (c'). It is found that the surface has changed from shiny metallic luster to colorful (brown color), which is different from that of TiN coatings usually appearing as golden [31, 32]. The reason for the presence of brown or golden color on the surface of cemented carbides is attributed to the influence of C content permeating into the Ti-containing surface on the cemented carbides. Moreover, the greater the carbon content infiltrates into the Ti-containing coating, the higher its hardness is, and the deeper color its surface appears [33]. Though the surface of as-carbonitriding specimen is still smooth, its roughness slightly decreases. By comparing the surface roughness of before and after carbonitriding specimen, it finds that the process of carbonitriding treatment can induce the surface roughness to decrease, which is consistent with the previous literatures [19, 20]. The C enriched alloy with larger grains having more planar surfaces and more triangular shape by comparing two alloys (C deficient and C enriched) shape change of the WC grains [19]. The Ti-containing skin layer is closely bonded on the WC-Co substrate. Due to the preferred orientation of grain growth, WC grains tend to abnormally growth. Most of WC grains forming under this condition are tabular crystal, their grain size is about 4  $\mu\text{m}$  and their thickness of the tabular crystal is about 1  $\mu\text{m}$ . TiN and N-diamond phases diffuse around or on WC grains, the grains size for TiN phases are nanoscale within a range of 500-800 nm. By comparing the above figures, we observe that the Ti-containing skin almost cover the surface of specimen completely. The reason for existing a few uncovering zones near or on WC tabular crystal grains is attributed to two factors: the first one is related to the low Ti content, and all specimens used in this study only add 0.5 wt.% Ti-containing. Thus it forecasts that the quality of skin layer can be improved with the increasing Ti element content. Another one

is attributed to the crystal orientation of WC grains. Preferential orientation relationships are frequently found at WC basal facets for WC/Co interfaces especially in the W enriched alloy [20].

## XRD analysis

### Phase identification

The composition and phase identification was performed on diffraction patterns. A continuous scanning mode ( $\lambda_{\text{Cu}, \text{K}\alpha} = 0.15406 \text{ nm}$ ) was used for testing these parameters within positions  $2\theta = 20.0^\circ - 90.0^\circ$ . The step size is 0.0330 and the scan step time is 4.8100 s. Two XRD diffraction patterns corresponding to the as-sintering specimen in vacuum and the as-carbonitriding specimen in nitrogen were obtained, respectively.

Primary WC phases including some metal binders such as Co, Mo and Ni phases are found in the Co capping as shown in Fig. 2 (a). Some diffraction peaks such as (100), (101) and (001) crystal planes are higher than the others. Moreover, Mo diffraction peaks such as (110) and (200) are obvious, which attributes to two factors: one is the relative sufficient Mo addition content (3.0 wt.%), another one is all specimens sintering in a Mo holder probably contributing more Mo diffusing into the surface of specimens. No Ti-containing phases can be found in this diffraction spectrum though existing TiC (0.5 wt.%) content in raw powders. The

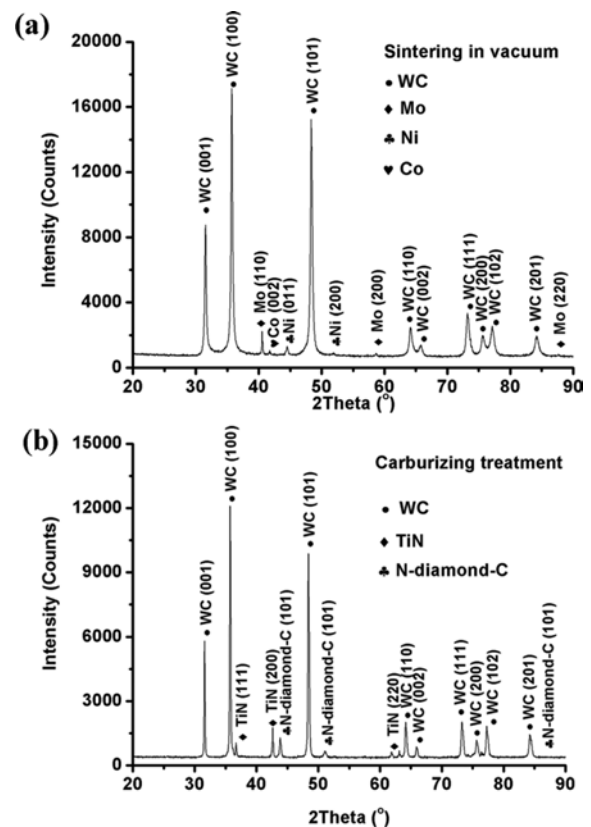


**Fig. 2.** XRD diffraction patterns for the as-sintering specimen in vacuum and the as-carburizing specimen in nitrogen, (a) sintering in vacuum, (b) carbonitriding treatment.

phenomenon of Co-enriched and fcc-free cubic phases forming in the surface can be attributed to the liquid phase migration of binders, and it also proves that the inward Ti diffusion is accompanied with the outward diffusion of Co, Mo and Ni binders. A functionally graded cemented tungsten carbide material (FG-WC-Co) is created with a gradient of structure such as materials composition, structure and grains size. A thick Co-capping layer mainly including Co, Mo and Ni binders is formed on the surface of the specimen, and is about 15-20  $\mu\text{m}$  its thickness. A layer mainly owning binders and no cubic carbides (WC, TiC, TiN and TiCN) existing in the zone, is located under the Co-capping layer, its grain size is about 5-10  $\mu\text{m}$ , and its grain growth appeared to be a columnar. A substrate layer having fine-grains WC phases with about 3  $\mu\text{m}$  grains size is then formed under the Co-capping layer. The preferred orientation of crystal growth in substrate was not obvious in comparison with the Co-capping layer. Therefore, it can be concluded that the whole structure possesses two layers with a graded structure characterized by a upmost Co capping with high Co, Mo and Ni binders, and a substrate layer with low Co content but high WC phases and no  $\eta\text{-Co}_3\text{W}_3\text{C}$  phases. Compared to conventional homogeneous WC-Co, FG-WC-Co has been found to be able to offer superior combinations of wear resistance and fracture toughness, as well as superior adhesive strength between coating and substrate [14].

After carbonitriding treatment some new phases form in the surface of specimen as shown in Fig. 2 (b). An obvious graded structure owning two layers was also formed on the in-situ surface of specimen after being post-sintering carbonitriding treatment. The outmost layer is the surface layer mainly containing high hardness and high wear resistance phases such as TiN, N-diamond C and sub-stoichiometric Co content, and now its color changes to brown and its thickness is about 1  $\mu\text{m}$ . The sub-layer is the substrate mainly including the WC phases and normal stoichiometric Co content. It is found that no microcracks emerge from the interface between the Ti-containing skin and substrate, and no obvious Ti-containing coatings peel or delaminate from substrate. So it concludes that the bonding interface between skin and substrate is fine and its adhesive strength is high. By comparing two diagrams, it finds that the former has a wider and higher WC diffraction peak but the latter owns a narrower and lower one. It indicates that the WC grain size has been changed before and after carbonitriding treatment. Moreover, the WC grain size slightly increases and its crystal status is also improved for the better after carbonitriding treatment. It is very important for cemented carbides to own fine WC grain and crystal growing pattern because that they are the base of possessing superior mechanical performance for cemented carbides [34]. The increasing in WC

grains size is attributed to the heat treating temperature at 1300  $^{\circ}\text{C}$ , which is higher than the three-phase-region temperature (solid Co, liquid Co and WC phases) at 1275  $^{\circ}\text{C}$ . So following the liquid phase migration of molten Co, Mo and Ni binders, most of the interfaces between WC grains can be adjusted to allow the WC grains to be re-orientated, which results in the WC grains slightly increasing. On the other hand, the process of carburizing heat treatment can reduce the defects such micro-cracks, micro-segregation or non-uniform for interior phases and holes in WC-Co, and greatly improve the compactness, density, surface hardness and mechanical performance of cemented carbide [35].

#### Residual stress analysis

Based on the foregoing XRD analysis for as-carbonitriding cemented carbides, we can obtain the continuous scanning spectrum of Ti-containing skin and the diffraction peaks for different phases after carbonitriding treatment. Since the TiN diffraction peaks such as (111) and (220) are too low to use to measure the residual stress of the Ti-containing skin, therefore the TiN (200) is used to evaluate that because of the ideal signal to noise ratio for TiN (200). The X-ray penetration depth is approximately 2  $\mu\text{m}$  with 50% of the diffracted intensity scattered from a layer extending to the penetration depth. The lattice parameter of TiN without residual stress is  $a = 0.4270$  nm, and the crystal plane spacing of TiN (200) is 0.1510 nm, the region of testing residual stress is located in the center of specimen during scanning process, and the spot size is controlled within 1 mm $\times$ 1 mm. Five incident angles ( $\psi = 0^{\circ}, 20.7^{\circ}, 30^{\circ}, 37.8^{\circ}$  and  $45^{\circ}$ ) are applied to test the residual stress in the skin, i.e. the increment  $\sin^2\psi$  is 0.125. Since every incident angle is induced by the different TiN (200) crystal plane orientation, the  $2\theta_{\psi}$  can reflect the change of TiN (200) crystal plane spacing  $d$ . The relationship between  $2\theta_{\psi}$  and  $\sin^2\psi$  is shown in Fig. 3. The slope of the line corresponding to  $2\theta_{\psi}\text{-}\sin^2\psi$  is then obtained using the least square method. The pressure stress generates when the slope  $L$  is greater than zero, and tension stress in turn forms when the slope  $L$  less than zero. The residual stress is calculated by the following equation [36].

$$\sigma_{\text{co}} = -\frac{E_{\text{co}}}{2(1+\mu_{\text{co}})} \cdot \cot\theta_0 \cdot \frac{\pi}{180} \cdot \frac{\partial(2\theta)}{(\sin^2\psi)} \quad (1)$$

where  $E_f = 450$  GPa is the elastic modulus of TiN film, and  $\mu_f = 0.21$  is its Poisson' ratio.

The red fitted line reflects the linear relationship between  $2\theta_{\psi}$  and  $\sin^2\psi$  for Ti-containing skin in the surface of specimen, and its slope also indicates the variation trend for the TiN crystal plane spacing ( $d$ ) changing with the diffraction angle  $\psi$ . Here the  $2\theta_{\psi}$  results increase with the increasing  $\sin^2\psi$  values, and

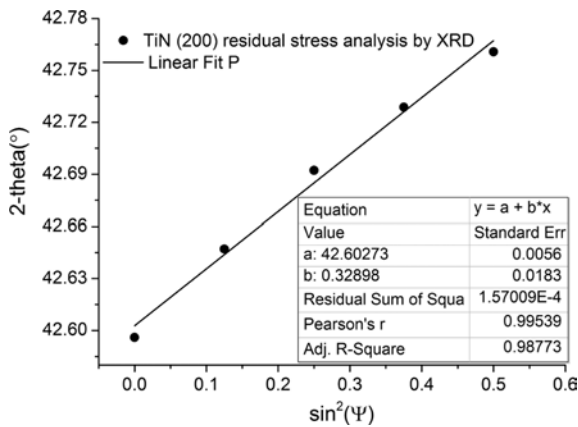


Fig. 3. The relationship between  $2\theta_\psi$  and  $\sin^2\psi$  for calculating residual stress.

the  $d$  values inversely decrease. The linear relationship between  $2\theta_\psi$  and  $\sin^2\psi$  is obvious, and its linear correlation coefficient is higher than 0.995, which indicates that the residual stress in Ti-containing skin is in a ideal plane stress state. The slope is about 0.3290 and pressure stress generates in the Ti-containing skin. Then the results such as the slope  $L = 0.3290$ , elastic modulus  $E_f = 450$  GPa and Poisson's ratio  $\mu_f = 0.23$  were all substituted into the equation (1), the pressure stress in Ti-containing skin of cemented carbides was calculated to be 1.18 GPa, which was consistent with other literatures [22, 23, 26, 37, 38]. Lyashenko *et al* [37] deposited the 2.0-10.5  $\mu\text{m}$  thick TiN coatings on 304 stainless steel by IBCM (Ion bombardment conditions method). Residual stresses in TiN coatings determined by curvature method changed from  $-0.78$  to  $-2.80$  GPa depending on the coating thickness. It was found that residual compression stresses increased to a maximum at 8  $\mu\text{m}$  thickness, then decreases rapidly, which may be attributed to the stress relaxation in the coatings. The residual stresses in all TiCN coatings are compressive and increase linearly with increasing C content in the coatings, moreover, with increasing C content in the coatings from 0 to 9.3 at.%, the residual stresses in the TiCN coatings increase continuously from 2.2 to 3.8 GPa [22, 23]. Larsson and Odén [26] determined the thermal residual stresses that develop in a functionally graded WC-Co composite by X-ray diffraction. Stresses were measured in both WC and Co phases at various depths. The result revealed that the in-plane compressive residual stresses for WC phases varied approximately between 300 and 500 MPa with depth below the surface, and the tensile residual stresses for the low volume fraction Co phase were about 600 MPa. Moreover, no significant macrostresses can be measured in a comparable homogeneous sample, i.e., without the compositional gradient. The residual compression stresses of TiN coatings with 0.2-1.7  $\mu\text{m}$  thickness changed from  $-5.93$  to  $-2.70$  GPa and decreased with the thickness [38]. The change of

residual stresses with the thickness is attributed to the preferred orientation of TiN (110) crystal plane, which results in the stress relaxation in the coating.

The residual stresses measured in this study are slightly lower than that reported in other literatures. The reason of owning lower residual stress may be attributed to the following factors: one is the different deposited technology. As you see in the foregoing sections, the specimen used in this study is covered by C graphite powers and sintered in nitrogen, therefore, the Ti-containing skin is obtained by chemical reactions between Ti atoms and N atoms in the surface of specimen. This kind of in-site crystal growing mode usually contributes to form lower residual stress because of the little differences in the thermophysical properties and graded structures between the skin and the substrate.

### Wear characteristics

The tool end-life criterion can be evaluated by friction coefficient, which is closely connected with the wear failure of cemented carbide. If the surface of cemented carbide is enough hard, its friction coefficient will mildly change. Its friction coefficient, in turn, will vary greatly, even appears a saltation. The friction test results for the as-sintered specimens before and after carbonitriding treatment reveal the change of friction coefficient and an increase in the lifetime of cemented carbide by carbonitriding treatment as shown in Fig. 4. The whole test time was 600 s for all specimens, the load was 200 g, the rotate speed was 300 r/min, and a  $\text{Si}_3\text{N}_4$  ceramic ball was applied as the milled balls.

As it is shown in this figure, two curves indicate that the friction coefficients of different surfaces change with test time or friction distance. The red one corresponding to the friction coefficient of the as-sintering specimen in vacuum is in the range of 0.32-0.5 before 320 s, and then it rapidly increases to 0.5-0.8 after 320 s, and the point at 320 s is a turning point. The blue one corresponding to the friction coefficient of the as-carbonitriding specimen in nitrogen changes slowly and keeps in the range of

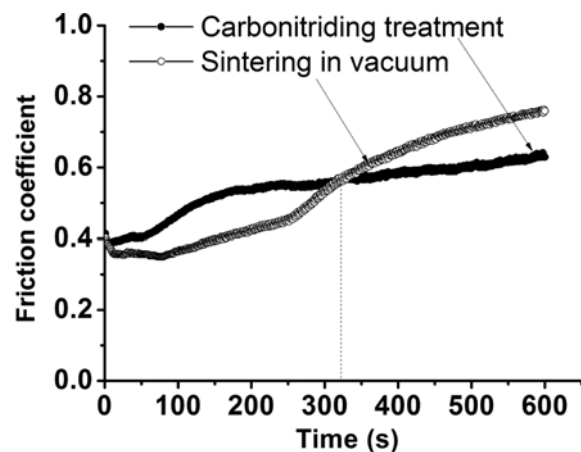


Fig. 4. Friction coefficients as a function of testing time.

0.4-0.6 during the whole 600 s test time. It is obvious that the changed range of the former is much higher than that of the latter. It also indicates that the latter has better wear resistance than the former because of the relative narrower changed range for the latter. Before 320 s, owing to lower friction coefficient of the former is attributed to the formation of ductile Co-capping layer on surface of specimen after sintering in vacuum. The red curve has a saltation at 250 s, which attributes to the specimen began to failure at this time, and the Co-capping layer began to crack or peel, so the friction coefficient rapidly increased with the increasing test time. Comparing with the red curve, the blue one changes mildly, and the reason for that is the formation of the Ti-containing hard skin in the surface of specimen after carbonitriding treatment, which has more superior wear resistance. Moreover, there are some N-diamond C phases existing in this skin, and C content usually influences on the friction coefficient of cemented carbides. The increasing C content in the TiCN coating led to a rapid decrease in the friction coefficient, and the increase in the C content in the TiCN coatings also resulted in a significant decrease in the wear rate of the TiCN coatings [22, 23]. So it is also concluded that the carbonitriding treatment can also improve the tool lifetime of cemented carbides.

### Conclusions

A Co-capping layer with 15-20  $\mu\text{m}$  thickness was obtained by sintering specimen in high vacuum ( $10^{-4}$  Pa), and a type of dome-like structure or hill-like structure was formed on this continuous Co-enriched and fcc-free cubic phase region. The Co-capping can be usually used to heal the defects such as pores and cracks in the surface of specimen and improve its surface toughness. Carbonitriding treatment resulted in the formation of fine-grained TiN phases and N-diamond C phases on the in-situ surface. It was concluded that carbonitriding treatment can be used to reduce the grain size and increase microstrains in the Ti-containing phases, and resulted in the formation of Ti-containing hard skin in the surface of specimen. The Ti-containing skin was brown and had high bond strength with the WC-Co substrate. There was a compression stress state remaining in Ti-containing skin and its residual stress was about 1.18 GPa. The carbonitriding treatment could improve the wear resistance of WC-Co.

### Acknowledgments

This paper is supported by the National Natural Science Foundation of China (61106124), Natural Science Foundation of Guangdong Province (S2013 010013385), Science and Technology or Industrial Research Projects of Zhanjiang City (2012D01, 2013 D01) and Program for Innovative Research Team in Zhanjiang Normal University (ZSIT13006).

### References

1. R. Frykholm, B. Jansson, H.-O. Andren, *Int. J. Refract. Met Hard Mater.* 20 (2002) 345-353.
2. R. van der Merwe, N. Sacks, *Int. J. Refract. Met Hard Mater.* 41 (2013) 94-102.
3. V. Bonache, M.D. Salvador, A. Fernández, A. Borrell, *Int. J. Refract. Met. Hard Mater.* 29 [2] (2011) 202-208.
4. R.M. Genga, L.A. Cornish, G. Akdogan, *Int. J. Refract. Met. Hard Mater.* 41 (2013) 12-21.
5. X.-y. Ren, Z.-j. Peng, Y. Peng, Z.-q. Fu, C.-b. Wang, L.-h. Qi, H.-z. Miao, *Int. J. Refract. Met. Hard Mater.* 36 (2013) 294-299.
6. N. Lin, C.-h. Wu, Y.-h. He, D.-f. Zhang, *Int. J. Refract. Met. Hard Mater.* 30 [1] (2012) 107-113.
7. M. Aristizabal, N. Rodriguez, F. Ibarreta, J.M. Sanchez, *Int. J. Refract. Met. Hard Mater.* 28 [4] (2010) 516-522.
8. José Garcia, *Int. J. Refract. Met Hard Mater.* 30 [1] (2012) 114-120
9. F. Xu, J.-H. Xu, M.-F. Yuen, L. Zheng, W.-Z. Lu, D.-W. Zuo, *Diam. Rel. Mater.* 34 (2013) 70-75.
10. Jiri Nohava, Pascal Dessarzin, Pavla Karvankova, Marcus Morstein, *Trib. Int.* 81 (2015) 231-239.
11. J.-F. Su, D. Yu, X. Nie, H. Hu, *Surf. Coat. Techn.* 206 [7] (2011) 1998-2004.
12. Y.-x. Qiu, S. Zhang, J.-w. Lee, B. Li, Y.-x. Wang, D.-l. Zhao, D. Sun, *J. Alloys Comp.* 618 (2015) 132-138.
13. X. Wang, Kyu Sup Hwang, Mark Koopman, L.-h. Zhang, *Int. J. Refract. Met. Hard Mater.* 36 (2013) 46-51.
14. P. Fan, Z. Zak Fang, J. Guo, *Int. J. Refract. Met. Hard Mater.* 36 (2013) 2-9.
15. L. Tahvilian, Z. Zak Fang, *Mate. Sci. Eng. A.* 557 (2012) 106-112.
16. P. Fan, J. Guo, Z.-g. Zak Fang, P. Prichard, *Int. J. Refract. Met. Hard Mater.* 27 [2] (2009) 256-260.
17. J. Guo, P. Fan, X. Wang, Z.-g. Zak Fang, *Int. J. Refract. Met. Hard Mater.* 28 [3] (2010) 317-323.
18. Peng Fan, Oladapo O. Eso, Zhigang Zak Fang, H.Y. Sohn, *Int. J. Refract. Met. Hard Mater.* 26 [2] (2008) 98-105.
19. I. Borgh, P. Hedström, T. Persson, J. Ågren, J. Odqvist, *Int. J. Refract. Met. Hard Mater.* 43 (2014) 205-211.
20. V. Bounhoure, S. Lay, F. Charlot, E. Pauty, J. M. Missiaen, *Int. J. Refr. Met. Hard Mater.* 44 (2014) 27-34.
21. C. Barbatti, J. Garcia, F. Sket, A. Kostka, A.R. Pyzalla, *Surf. Coat. Techn.* 202 (2008) 5962-5975.
22. Y.-H. Cheng, T. Browne, B. Heckerman, *Vac.* 85 [1] (2010) 89-94.
23. Y.-H. Cheng, T. Browne, B. Heckerman, E.I. Meletis, *Surf. Coat. Techn.* 205 [16] (2011) 4024-4029.
24. H.K. Tönshoff, A. Mohlfeld, C. Gey, J. Winkler, *Surf. Coat. Techn.* 108-109 (1998) 543-550.
25. T. Sato, Y. Hosokawa, S. Ito, K. Akashi, *Surf. Coat. Techn.* 112 (1999) 189-193.
26. C. Larsson, M. Odén, *Int. J. Refr. Met. Hard Mater.* 22 (2004) 177-184.
27. D.S. Janisch, W. Lengauer, K. Dreyer, H. van den Berg, in *Proc. 17th Plansee Seminar, May 2009*, 2: p. 52.
28. E. Sachet, W.D. Schubert, G. Mühlbauer, J. Yukimura, Y. Kubo, *Int. J. Refr. Met. Hard Mater.* 31 (2012) 96-108.
29. I. Konyashin, *Vac Sci. Technol. A.* 14 [2] (1996) 447-52.
30. I. Konyashin, *Funct Mater.* 1 (1994) 106-10.
31. J. Kraft, O. Rattunde, O. Rusu, A. Häfele, H. Haberland, *Surf. Coat. Techn.* 158-159 (2002) 131-135.
32. C.-M. Lee, J.-P. Chu, W.-Z. Chang, J.-W. Lee, J.-S. C.

- Jang, P.-K. Liaw, *Thin Solid Films*. 561 (2014) 33-37.
33. S.-W Huang, M.-W Ng, M. Samandi, M. Brandt, *Wear*. 252 [7-8] (2002) 566-579.
34. X.-q.Li, J. Chen, D.-h. Zheng, S.-g. Qu, Z.-y. Xiao, *J.Alloys Comp.* 544 (2012) 134-140.
35. A.F.Lisovsky, *Int. J. Heat Mass Transfer*. 33 (1990) 1599-603.
36. M.-f. Gong, S.-r. Qiao, G.-f. Lu, H. Ji, B.A. Lyashenko, *China J. Mech. Engin.*46 [6] (2010) 100-107.
37. B.A. Lyashenko, A.V. Rutkovskii, E.B. Soroka, N.V. Lipinskaya, *Strength Mater.* 33 [4] (2001) 344-349.
38. W.-J. Chou, G.-P.Yu, J.-H. Huang, *Surf. Coat. Techn.* 149 (2002) 7-13.
39. X.-y. Song, Y. Gao, X.-m. Liu, C.-b. Wei, H.-b. Wang, W.-h. Xu, *Acta Materi.* 61 [6] (2013) 2154-2162.